APPENDIX 6.E. ONE DIMENSIONAL SUBSIDENCE MODELING

Prepared as part of the

Joint Groundwater Sustainability Plan
Madera Subbasin

January 2020
Amended January 2025

GSP Team:

Davids Engineering, Inc (Amended GSP Team)
Luhdorff & Scalmanini (Amended GSP Team
ERA Economics
Stillwater Sciences and
California State University, Sacramento

Luhdorff & Scalmanini
Consulting Engineers

TECHNICAL MEMORANDUM

DATE: October 2, 2024 Project No. 24-1-010

TO: Madera Subbasin Joint GSP GSAs

FROM: LSCE

SUBJECT: One Dimensional Subsidence Modeling

1 INTRODUCTION

Land subsidence is a major concern in the San Joaquin Valley and is related to the use of groundwater to supplement variable surface water supplies. Subsidence has the potential to damage local, state, and federal infrastructure, including reducing the freeboard and flow capacity in irrigation water-delivery canals, bridges, roads, and flood control structures.

In alluvial depositional environments, fine-grained materials are generally arranged in laterally extensive and/or discontinuous confining units referred to as "interbeds" within an aquifer system. For the purposes of evaluating subsidence, the term "aquifer" refers to the water-bearing interconnected coarse-grained material within the aquifer system where (due to larger hydraulic diffusivity) the majority of initial water level and groundwater storage changes occur due to pumping.

Compaction and land subsidence are due to elastic and inelastic deformation of the aquifer skeleton (Terzaghi, 1925, **Figure 1**). As shown in Figure 1, a decrease in pore-water pressure (ρ) in a confined aquifer leads to an increase in effective stress (σ_e) and vertical displacement (μ_z). Inelastic deformation occurs predominantly in the fine-grained materials within an aquifer system (Ireland, 1984; Hanson, 1989). Inelastic deformation occurs in cases where the effective stress within the interbeds exceeds the greatest effective stress ever experienced within interbeds, which is referred to as "pre-consolidation stress" (Holzer, 1981). This is triggered when the hydraulic head in the interbeds drops below historic levels, referred to as "pre-consolidation head" (Jorgensen, 1980; Leake and Prudic, 1991; Hoffman et al., 2003). The pre-consolidation stress threshold is a combination of previous low groundwater levels (buoyant force) and any past increases in geologic loading from sedimentary deposition plus any potential lithification or cementation of the sediments that comprise the aquifer system. Inelastic deformation and compaction result in the irreversible rearrangement of the grains within the aquifer skeleton, leading to a permanent reduction in aquifer storage and compaction.

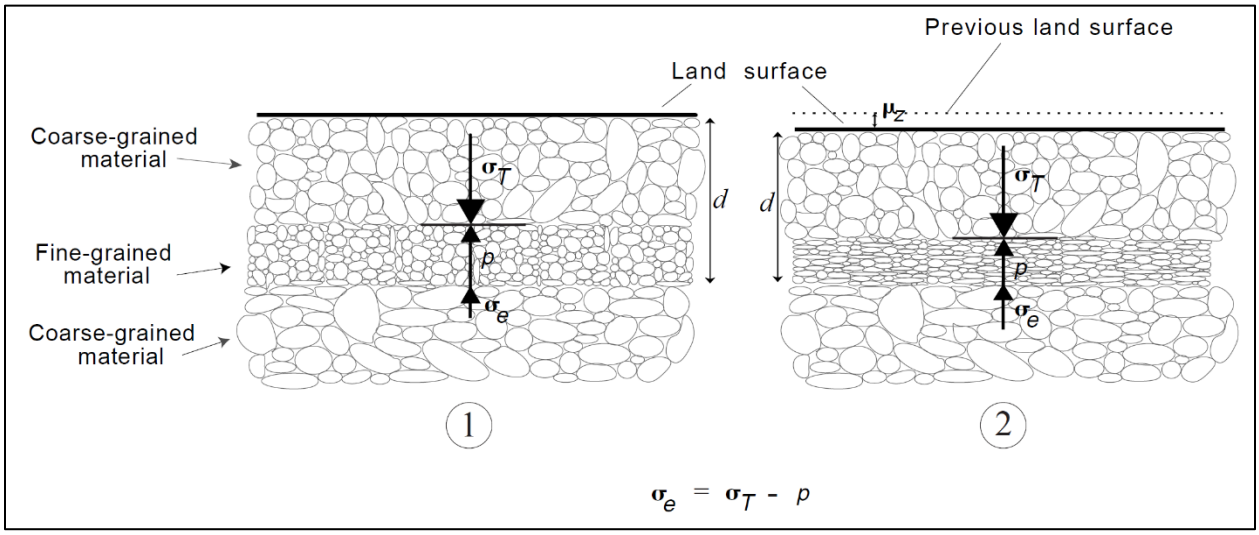

Source: Sneed and Galloway, 2000

Figure 1. Relationship between pore-water pressure, effective stress, and vertical displacement

Depending on the geometry (distribution and thickness) and hydraulic properties of the interbeds within an aquifer system; there may be a significant time delay for hydraulic heads within interbeds to equilibrate with heads in adjacent aquifers (Terzaghi, 1925). As a result, so-called "ultimate" or "residual" amounts of compaction may not be manifested until residual excess pore pressure in the interbeds is released, which can occur much later than the initial decline in water levels within the vertically adjacent aquifer. Recognition of this dynamic can be critical in slowly draining aquifer systems since the change in effective stress within interbeds (compaction) can continue to occur even when the measured hydraulic head within the aquifer does not exceed the pre-consolidation head as previous reductions of pore pressure from the adjacent aquifers are still propagating across the interior of the fine-grained beds (Sneed et al., 2018).

The goal of this study is to assess the component of residual subsidence contributing to total subsidence at two sites located within the Madera Subbasin (MW-5, MW-9), including how changes to projected groundwater levels resulting from implementation of the Sustainable Groundwater Management Act (SGMA) impact residual subsidence and the time delay in future subsidence if groundwater levels remained constant or increased.

2 APPROACH

The approach used to evaluate delayed aquitard drainage at MSB-05 (MW-5) and MSB-09 (MW-9) follows methodology established from previous efforts to numerically assess subsidence in the San Joaquin Valley (SJV) through a 1-dimensional (1D) compaction model (Helm, 1975, 1976; Lees, 2022). In general, these model approaches are built upon a conceptual model that in alluvial aquifer systems, such as occurs in the SJV, an aquitard-drainage model best describes subsidence due to the large-scale three-layered hydrostratigraphy in the SJV that contains: an upper aquifer, a regional confining layer (Corcoran Clay), and a lower aquifer. The upper and lower aquifers are of mixed, alluvial systems with interlayered coarse and fine-grained (clay) material, which is subject to inelastic compaction. When groundwater levels

decline, the aquifer system experiences a drop in hydraulic head asynchronously. Head drops first in coarse-grained materials in the upper and lower aquifers, while head in the Corcoran Clay and clay interbeds responds gradually due to a much lower vertical hydraulic conductivity, resulting in a process called delayed aquitard drainage (or "residual" subsidence).

In a 1D compaction model, changes in the hydraulic head within coarser-grained sediments are considered known, either through direct measurement or simulation. The model then subsequently determines the gradual drainage of the clay interbeds and the confining layers separating the interbeds and calculates the resulting compaction from decreases in the hydraulic head. Thus, the model can be applied to simulate both compaction in multilayered aquifer systems and the residual compaction of clays within the aquifer(s).

Residual subsidence in a 1-D aquitard drainage model can be simulated with MODFLOW, which employs a finite difference model method that uses a finite difference representation of vertical stress distribution to simulate subsidence by coupling fluid flow with changes in pore pressure and deformation of geologic material.

For this model, we used textural data taken from MW-5 and MW-9 to assign depth intervals of coarse and fine sediment units based on an ohms per meter (ohm-m) threshold value from the short-normal resistivity log response. Seasonal water level measurements from both MW-5 and MW-9 from 2020–2024, and historical water level data from wells in the nearby vicinity, were used as hydraulic head inputs. Regional InSAR data and measured subsidence data were used as observed subsidence inputs.

3 MODEL PLATFORM

The One-Water Hydrologic Flow Model (One-Water) is an integrated hydrologic flow modeling software developed by the USGS to evaluate three-dimensional groundwater flow (Boyce et al., 2020). Additionally, One-Water integrates various processes and packages to enable the robust and dynamic simulation of landscape supply and demand, groundwater-surface water interaction, and groundwater flow, which was not used in this study. Similar to previous versions of MODFLOW, One-Water is a three-dimensional, finite difference modeling code that utilizes the concept of modularization to represent various aspects of the hydrologic system (McDonald and Harbaugh, 1988). Modularization is represented by individual model code packages that simulate different hydrologic processes that occur in groundwater basins.

4 MODEL PACKAGES

The components of the model (model packages) utilized in the model are described below.

Basic Package: The MODFLOW Basic (BAS) package specifies the location of active and inactive model cells and initial heads used at the start of the simulation (Harbaugh et al., 2000).

Discretization Package: The MODFLOW Discretization (DIS) package specifies the spatial and temporal model geometry. The spatial discretization includes the row and column spacing and model cell top and bottom elevations. The temporal discretization includes the number and length of model stress periods and timesteps. A MODFLOW stress period is a length of time where specified model stresses are constant. A stress period may be broken up into one or more timesteps for which flow equations are solved (Harbaugh et al., 2000).

Output Control Package: The Output Control (OC) package specifies the printing of simulated groundwater heads and volumetric budget (Harbaugh et al., 2000).

Newton Solver: The Newton (NWT) solver is a method for solving the system of equations used to approximate the groundwater flow equation through finite differences. The NWT solver provides a robust method for solving nonlinear problems, which include unconfined groundwater flow and cell drying and rewetting (Niswonger et al., 2011).

Upstream Weighting Package: The Upstream Weighting (UPW) package specifies the hydraulic properties within model cells. These include horizontal hydraulic conductivity, vertical hydraulic conductivity, specific yield, and specific storage (Niswonger et al., 2011).

General-Head Boundary Package: The General-Head Boundary (GHB) package is a head-dependent flux boundary condition used to simulate lateral subsurface flow into and out of the model domain from large water bodies (Harbaugh et al., 2000). The flux between a model cell and a GHB cell is calculated based on the hydraulic head in the model and GHB cell and the conductance specified between them.

Subsidence Package: The Subsidence (SUB) package is used to simulate changes in groundwater storage and compaction of aquifer systems (Hoffman et al., 2003). The SUB package accounts for elastic and inelastic storage changes due to the deformation of the aquifer system in confined aquifers based on the pre-consolidation head.

5 MODEL DEVELOPMENT

Data sources

This section describes input data utilized for model development at MW-5 and MW-9. Textural data was used to define intervals of coarse-and-fine-grained sediments, water level data was used for hydraulic head inputs, and observed subsidence was used to calibrate and evaluate model outputs.

Textural data

During the installation of MW-5 and MW-9 in the Fall of 2019, a suite of geophysical logging tools was deployed down the boreholes. Included within the suite are resistivity observations, measured in ohms per meter (ohm-m), from the short-normal resistivity curve response and a reported textural log that textually and graphically illustrates sediment material as either coarse or fine. Resistivity observations and textural interpretations were used in conjunction to develop discrete intervals of fine and coarse-grained sediments, which were then used as model inputs as aquifer or interbed layers.

Water Level Data

Water level data used was built from a composite of DWR wells within the vicinity of MW-5 and MW-9, and the water level transducer data recorded from MW-5 and MW-9 between the Fall/Winter of 2019 through the Spring of 2024.

Subsidence Data

Observed subsidence data were obtained from multiple sources for model sites MW-5 and MW-9, which included both field and geodetic measurements. Estimated subsidence from field measurements between 1926 and 1970 was acquired from Poland and others (1975). Geodetic measurements, such as interferometric synthetic aperture radar (InSAR), were used to estimate subsidence in the following data sources: NASA Jet Propulsion Laboratory (January 2007–January 2021; NASA JPL, 2018; Farr et al., 2015), PALSAR (July 2007–October 2010; Sandwell et al., 2008), RadarSat (May 2014–May 2015), and monthly measurements from TREAInSAR (July 2015–January 2024; Tre Altimira, 2021).

Model Discretization

The model's discretization defines the spatial boundaries of the modeled area, model layering, and model cell size, as well as the time series element of the simulation.

Spatial Discretization and Model Layering

The model domain for MW-5 and MW-9 is a finite difference grid of 1 row and 1 column that is essentially a single cell with a constant cell width along both columns and rows. The model was discretized vertically into 859 layers for MW-5 and 1,101 layers for MW-9, with a constant 1-foot layer thickness throughout all layers to accurately capture the thickness and total number of interbeds, including the Corcoran clay. The top of layer 1 represents the land surface, where the primary data source of land surface elevation was the reported ground surface elevation on the driller's log.

Temporal Discretization

The total time simulated using the numerical model for MW-5 and MW-9 starts in April 1921 through December 2070. The simulation period is divided into 1,797 monthly stress periods where groundwater levels are assigned and subdivided equally into 2 model timesteps for which hydraulic head and model fluxes are calculated.

Assigning Texture to Grid

To identify the thickness of clay interbeds and the Corcoran Clay at MW-5 and MW-9 model sites, this approach used a binary textural classification of digitized resistivity logs and reported drillers textural logs to assign layers with coarse-grained (sands, gravels, clayey sands) or fine-grained (clay, silt, sandy clays) sediments. We interpreted the resistivity log by identifying fine-grained sediments as the layer with the lowest resistivity, using a specific resistivity cutoff value to determine sediments presumed to be clay on the short-normal resistivity log and textural description. For each model layer, the mean short-normal resistivity value from a 1-foot interval was assigned to the layer as either fine (“aquitard” or interbed) or coarse-grained (“aquifer”) category, depending on the resistivity value. At the MW-5 site, we interpreted each 1-foot model layer with a log response of less than 17 ohm-m to be fine-grained interbeds, while at the MW-9 model site, the cut-off was 12 ohm-m.

Parameters

The parameters specified in the model for MW-5 and MW-9 sites are listed below. There are nine hydrologic parameters: vertical hydraulic conductivity of the aquitards and aquifers (denoted here as $K_{v\ aquitard}$ and $K_{v\ aquifer}$, respectively, and assigned in UPW), inelastic skeletal specific storage of aquitards and aquifers

(denoted here as $Ss_{kv\ aquitard}$ and $Ss_{kv\ aquifer}$, respectively and assigned in SUB), elastic skeletal specific storage of aquitards and aquifers (denoted here as $Ss_{ke\ aquitard}$ and $Ss_{ke\ aquifer}$, respectively and assigned in SUB), pre-consolidated head of the aquitards and aquifers (denoted here as $H_{pc\ aquitard}$ and $H_{pc\ aquifer}$ respectively and assigned in SUB), and specific yield of the aquitards and aquifer (denoted here as $S_{y\ aquitard}$ and $S_{y\ aquifer}$ respectively and assigned in UPW). The initial values used for these parameters were specified using corresponding values assigned in the Central Valley Hydrologic Model Version 2 (Traum and Faunt, 2022).

Assigning Water Levels to Aquifers

Water Level Zones

At MW-5 and MW-9 sites, the historical water level data from 1915–2024 was aggregated into 3 aquifer zones: the Upper Aquifer, the Lower Aquifer (shallow), and the Lower Aquifer (deep). The Corcoran Clay separates the upper aquifer and lower aquifer zones for both sites. The lower aquifer-deep zone interval is between 400–858 feet depth for MW-5 and 749–1,100 feet depth for MW-9.

General Head Boundary

Raw water level data from 1915–2024 for each of the three aquifer zones was then processed through a piecewise cubic hermite interpolating polynomial regression model, which was then used to obtain water level measurement estimates on a monthly frequency from January 1st, 1915, through December 31st, 2070. The interpolated data was then assigned to the GHB MODFLOW input package at depth intervals corresponding to the upper aquifer, the lower aquifer-shallow, and the lower aquifer-deep. Adjustments to aquifer-specific water levels, when only an unconfined water level is available, were achieved by evaluating estimates of vertical hydraulic gradients between the unconfined and respective confined aquifers.

Water Level Scenarios

To better understand how varying water level Scenarios can impact potential future residual subsidence, we developed three Scenarios that represent possible future water conditions at MW-5 and MW-9 (**Figures 2 and 3**):

Scenario 1: Extension of seasonal low measurement from 2022 and extending that value from 2024 through 2070 to represent constant groundwater levels

Scenario 2: (1) Extension of seasonal low measurement value from 2022 through 2030, (2) increasing water levels 20 feet from 2030 through 2040, and (3) extending stabilized water levels at 2040 levels through 2070

Scenario 3: (1) Extension of seasonal low measurement value from 2022 through 2030, (2) increasing water levels 20 feet from 2030 through 2040, (3) increasing water levels 20 feet from 2040 through 2055, (4) and then extending stabilized water levels at 2055 levels through 2070.

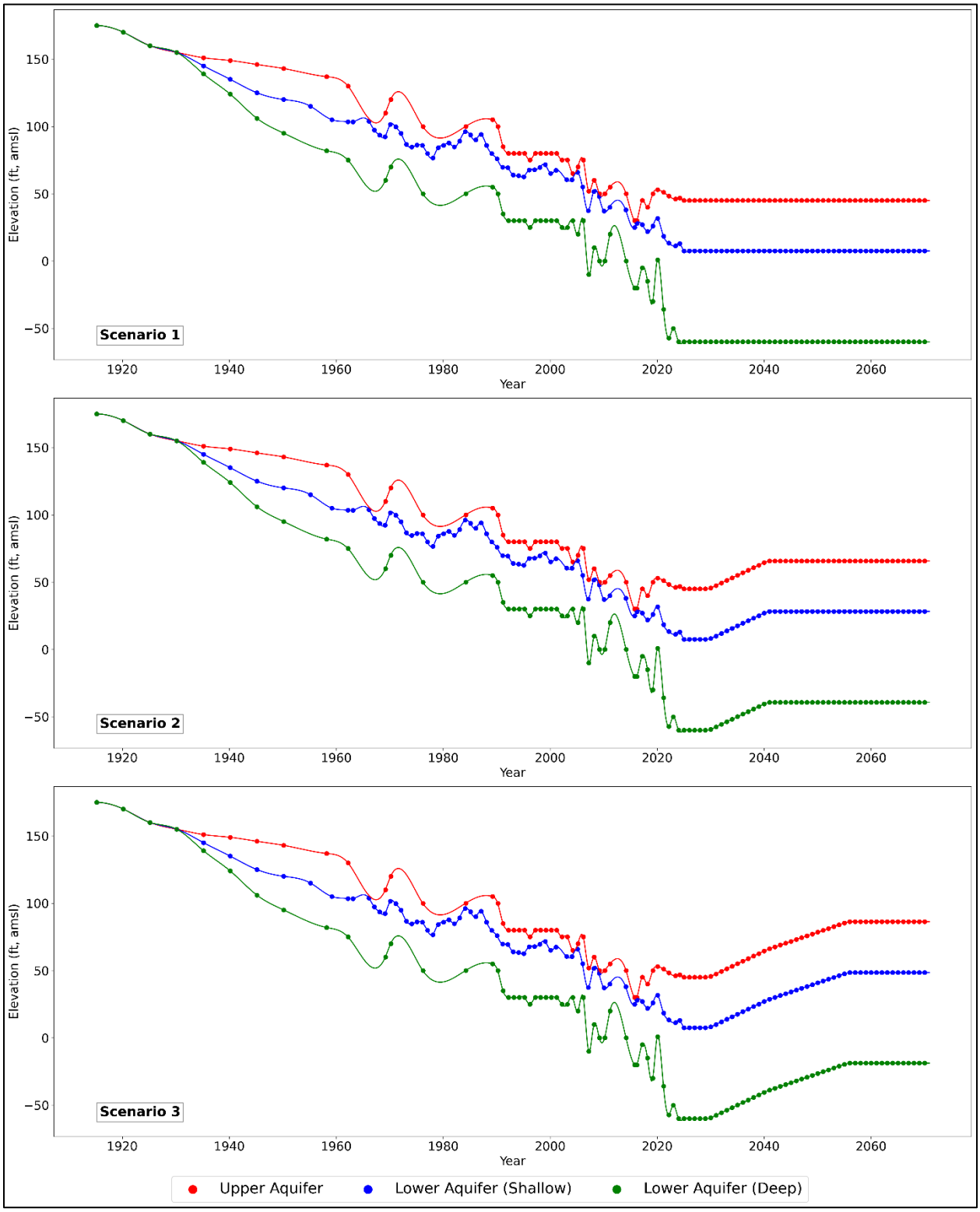

Figure 2. Groundwater levels assigned in Scenarios 1, 2, and 3 for MW-5

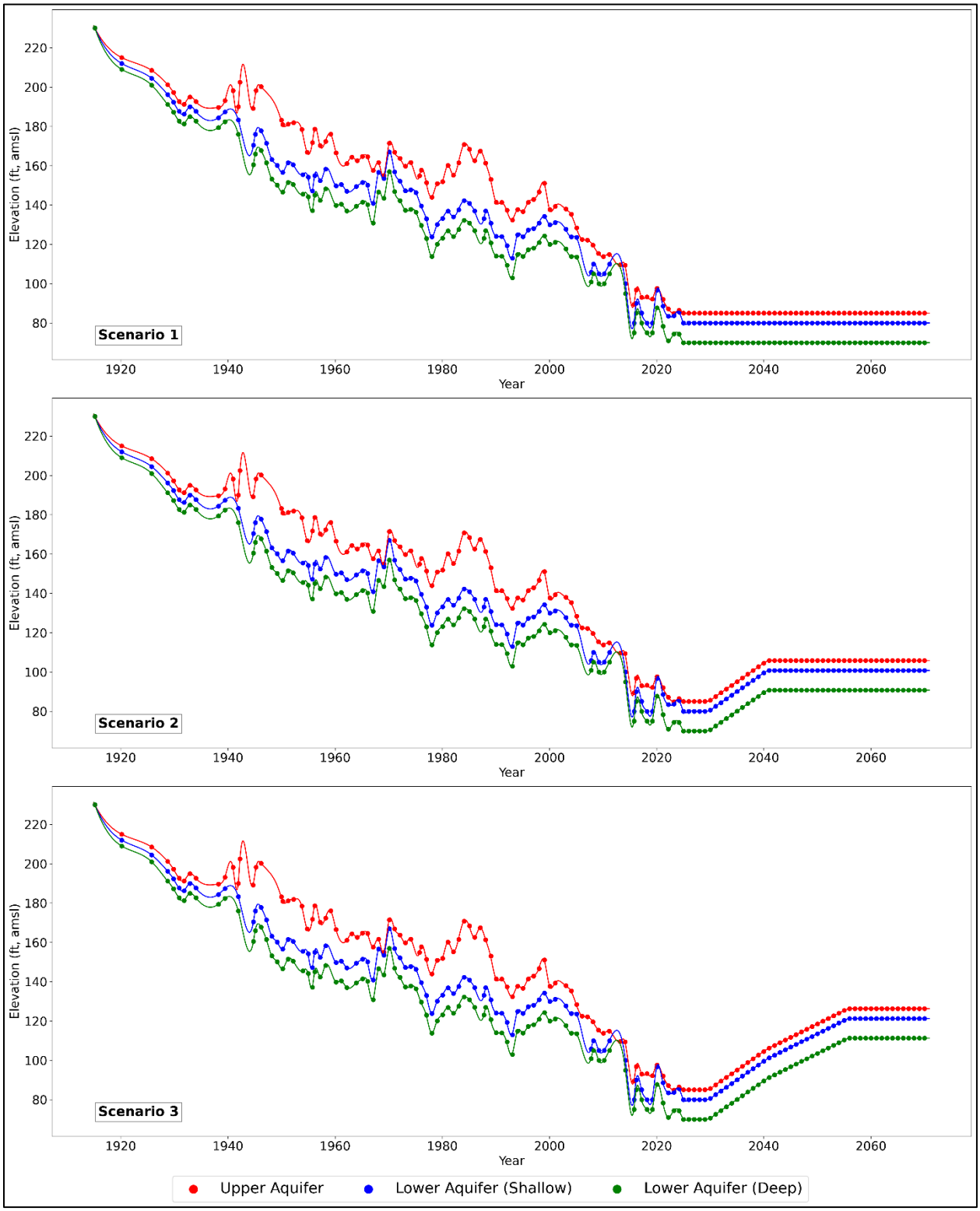

Figure 3. Groundwater levels assigned in Scenarios 1, 2, and 3 for MW-9

6 MODEL RESULTS

Calibration and Model Fit

The numerical model was calibrated through a combination of manual (trial-and-error) and automated (brute force) methods. Optimal parameter values were determined by parameter combinations that minimized the residual sum of squares (RSS):

$$RSS = \sum_{i=1}^{n}(\hat{y}_i - y_i)^2 \quad \text{(Equation 1)}$$

Where n is the total number of observations;

y_i is the ith observed value; and
$\hat{y}_i$ is the ith simulated value of a model-dependent variable.

The model was initially calibrated using manual trial and error methods using parameter values within the expected range for aquifer properties in the SJV (Faunt et al., 2009). Trial and error calibration was focused on matching the overall trend and magnitude of measured subsidence at each site. Trial and error calibration identified the parameters $K_{v\ aquitard}$ and $Ss_{kv\ aquitard}$, which had the greatest impact on the timing and magnitude of historical and projected subsidence. These parameters were selected for automated brute force optimization, which systematically tested combinations of these parameters to identify the "best" fit that minimizes the RSS.

The calibrated aquifer parameters used in the simulation of subsidence at MW-5 and MW-9 are shown in **Table 1**.

Table 1. Calibrated Parameters

Parameter Name	Parameter Value	
	MW-5	MW-9
$K_{v\ aquitard}$ (ft/d)	3.38×10^{-6}	3.38×10^{-6}
$Ss_{kv\ aquitard}$ (ft^{-1})	7.70×10^{-4}	8.00×10^{-5}

Model Fit at MW-5

The numerical model shows a generally agreeable fit to observed data from the various sources of measured subsidence at MW-5. Fit statistics, including the mean error (ME), mean absolute error (MAE), the sum of squared error (SSE), and root mean squared error (RMSE), are shown in **Table 2** (Anderson and Woessner, 1992). The model fit early subsidence (1926–1970), as reported by Poland and others (1975), is uncertain and was fit primarily by adjusting the pre-consolidation head in the lower aquifer. Total simulated subsidence over the historical period totals approximately 8 feet–a large portion of which occurred between 2007 and 2024 (**Figure 4**).

Table 2. MW-5 Fit Statistics				
Model	Statistic			
	Mean Error (ft)	Mean Absolute Error (ft)	Sum of Squared Error (ft^2)	Root Mean Squared Error (ft)
MW-5	-0.051	0.109	2.34	0.141

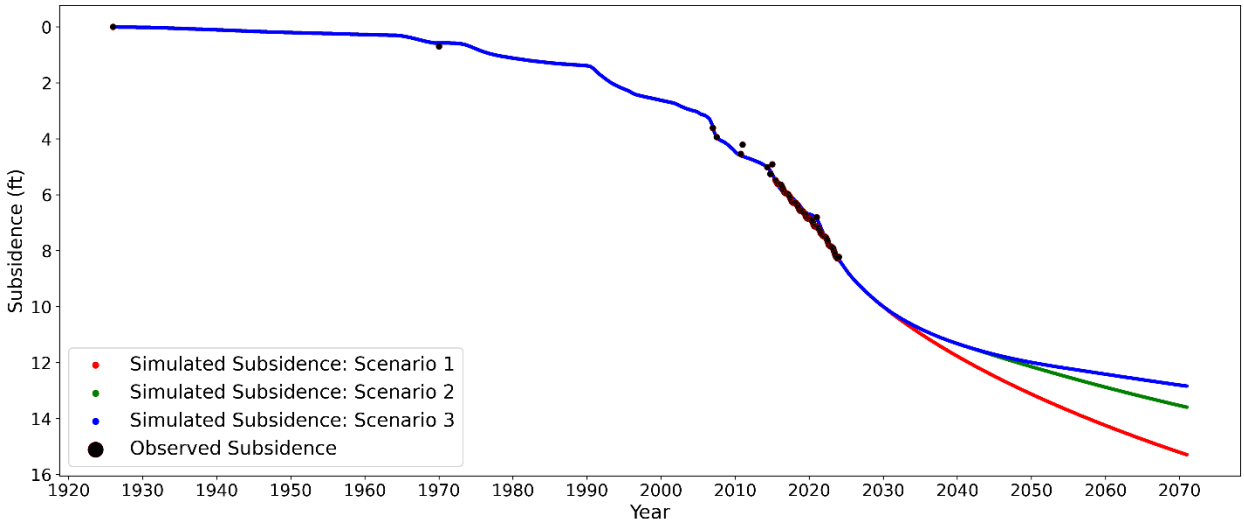

Figure 4. Simulated Subsidence at MW-5 (Historical and Projected Scenarios 1-3)

Model Fit at MW-9

The numerical model shows a generally agreeable fit to observed data from the various sources of measured subsidence at MW-9. Fit statistics, including the mean error (ME), mean absolute error (MAE), the sum of squared error (SSE), and root mean squared error (RMSE), are shown in **Table 3** (Anderson and Woessner, 1992). The model fit early subsidence (1926–1970), as reported by Poland and others (1975), is uncertain and was fit primarily by adjusting the pre-consolidation head in the lower aquifer. Total simulated subsidence over the historical period totals approximately 2.3 feet—about half of which occurred between 2007 and 2024 (**Figure 5**).

Table 3. MW-9 Fit Statistics				
Model	Statistic			
	Mean Error (ft)	Mean Absolute Error (ft)	Sum of Squared Error (ft^2)	Root Mean Squared Error (ft)
MW-9	0.053	0.061	0.537	0.069

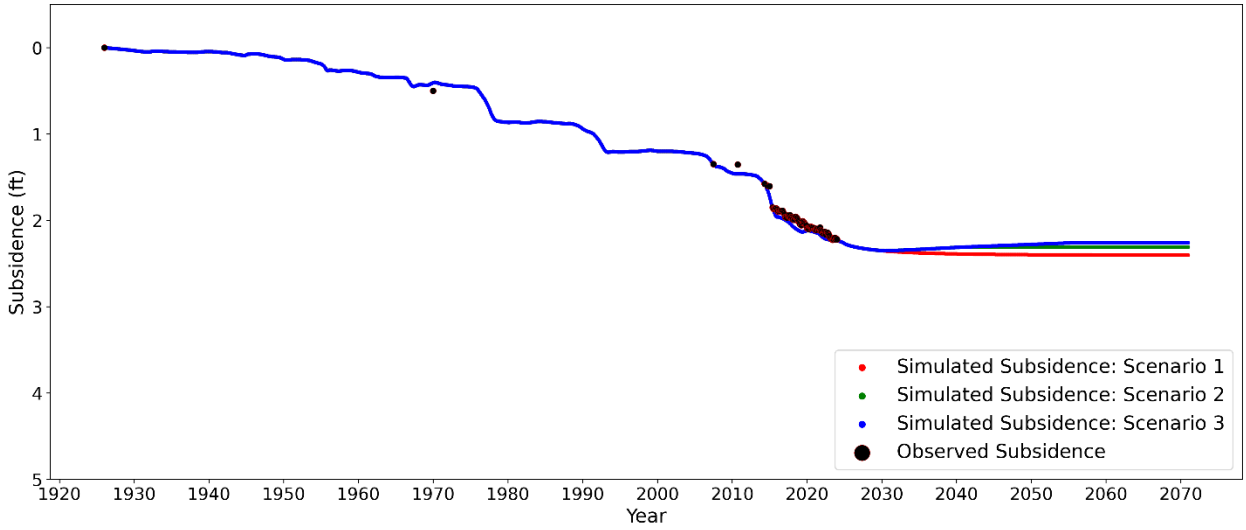

Figure 5. Simulated Subsidence at MW-9 (Historical and Projected Scenarios 1-3)

Projected Residual Subsidence

The numerical model was used to estimate residual subsidence at MW-5 and MW-9 under the projected water level Scenarios described in **Section 5**. A summary of the projected residual subsidence under these Scenarios is described below.

Residual Subsidence at MW-5

The variations between water level Scenarios primarily affect the rate of subsidence post-2024, with Scenario 1 (**Figure 4**) projecting the most future subsidence and Scenario 3 (**Figure 4**) the least. Overall, the model shows consistency across all water level Scenarios, being capable of consistently identifying periods of increased subsidence and gradual stabilization. Subsidence under water level Scenario 1 (**Table 4**) shows initial subsidence at 1.69 feet from 2024 to 2030, followed by an increase to 1.77 feet during the water level rise from 2030 to 2040, and then 1.35 feet in the next period (2040–2050), indicating a gradual slowing of the rate of residual subsidence under stable water levels over the entire period (2024–2070). Scenario 2 (**Table 4**) shows decreased rates of residual subsidence during periods of water level rise. In the initial period (2024–2030), subsidence is 1.68 feet, followed by 1.32 feet during increasing water levels from 2030 to 2040, and then further declines in rates of subsidence to 0.73 feet for 2050–2060, and 0.66 feet from 2060–2070. These fluctuations suggest that rates of residual subsidence decrease initially with rising water levels compared to stable water levels. Under Scenario 3 **(Table 4**), subsidence between 2024 to 2040 mirrors Scenario 2, but then residual subsidence rates are lower in the intermediate periods (2040–2060), where water levels are still rising, with values at 0.67 feet from 2040 to 2050 and at 0.42 feet from 2050 to 2060. As water levels stabilize, there is a further decline of 0.39 feet for 2060–2070. This indicates a more pronounced reduction in the rates of subsidence, especially during periods of increasing water levels, but that some amount of residual subsidence continues to occur.

Table 4. Simulated Residual Subsidence for MW-5			
Time Period	Simulated Subsidence		
	Scenario 1[1]	Scenario 2[2]	Scenario 3[3]
2024–2030	1.69	1.68	1.68
2030–2040	1.77 (3.45)[4]	1.32 (3.00)	1.32 (3.00)
2040–2050	1.35 (4.81)	0.82 (3.83)	0.67 (3.67)
2050–2060	1.12 (5.93)	0.73 (4.56)	0.42 (4.10)
2060–2070	0.96 (6.89)	0.66 (5.22)	0.39 (4.49)

1. Stable water levels
2. Water level increases in 2030–2040
3. Prolonged water level increases in 2030–2040 and 2040–2055
4. Cumulative subsidence

Residual Subsidence at MW-9

Subsidence estimates at MW-9 under Scenario 1 (**Table 5**) show subsidence at 0.11 feet for 2024–2030, 0.037 feet for 2030–2040, and 0.01 feet for 2040–2050 before reaching 0.0 feet for 2060–2070. Under Scenario 2 (**Table 5**), subsidence is estimated at 0.11 feet for 2024–2030, -0.04 feet during the period of rising water levels (2030–2040), and experiences no further appreciable increase or decrease for 2040-2070. This trend suggests that rising water levels in the intermediate period lead to a slight positive vertical displacement, which tapers off by 2070.

Subsidence estimates under Scenario 3 (**Table 5**) show subsidence at 0.112 feet for 2024–2030, decreasing by -0.0359 feet during the first rise (2030–2040), followed by a slight decline to -0.0348 feet and -0.0198 feet during the next time periods of 2040 to 2050 and 2050 to 2060, respectively. Subsidence stabilizes at 0 feet for 2060–2070. This Scenario shows the most significant positive vertical displacement during periods of rising water levels, but the effect slows as water levels stabilize in later years.

Table 5. Simulated Residual Subsidence for MW-9			
Time Period	Simulated Subsidence		
	Scenario 1[1]	Scenario 2[2]	Scenario 3[3]
2024–2030	0.11	0.11	0.11
2030–2040	0.037 (0.02)[4]	-0.04 (0.08)	-0.04 (0.08)
2040–2050	0.01 (0.160)	-0.00 (0.072)	-0.03 (0.0411)
2050–2060	0.0 (0.16)	0 (0.07)	-0.02 (0.021)
2060–2070	0.0 (0.16)	0 (0.07)	0 (0.02)

1. Stable water levels
2. Water level increases in 2030–2040
3. Prolonged water level increases in 2030–2040 and 2040–2055
4. Cumulative subsidence

Model Non-Uniqueness

Brute force calibration revealed correlation and non-uniqueness between the vertical hydraulic conductivity of the aquitard ($K_{v\ aquitard}$) and the skeletal storage coefficient of the aquitard ($Ss_{kv\ aquitard}$). Multiple parameter combinations produced a fit that minimized the error between observed and simulated subsidence. In MW-5, these combinations fell within previously reported estimates of $K_{v\ aquitard}$ and $Ss_{kv\ aquitard}$ summarized in Faunt and others (2009) and are shown in **Figure 6**. At MW-9, an agreeable model fit was only achieved at low $K_{v\ aquitard}$ and high $Ss_{kv\ aquitard}$ values within the previously estimated range.

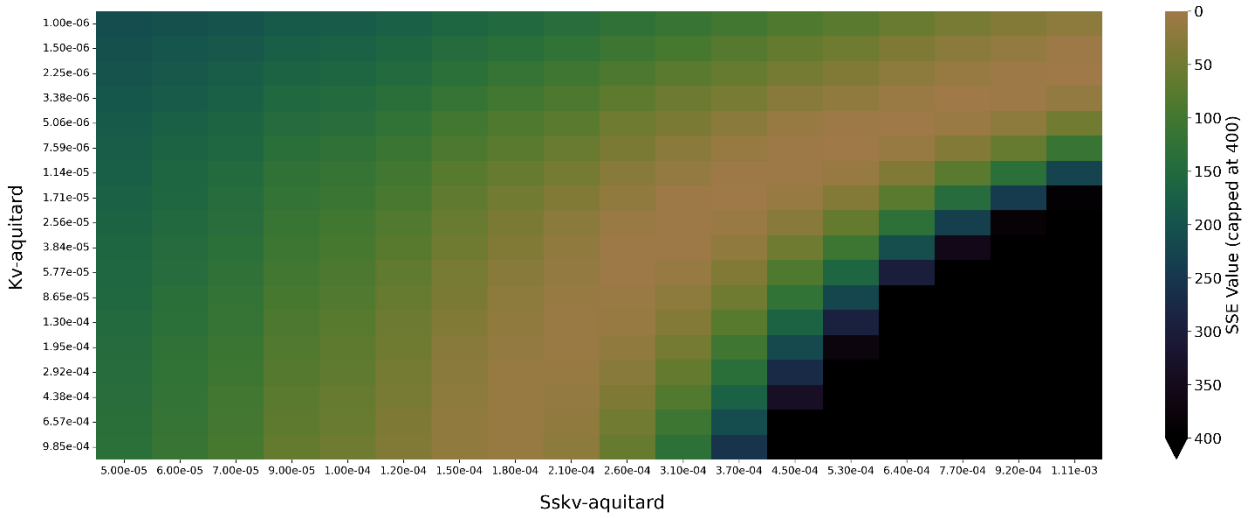

Figure 6. Error Surface at MW-5 for various parameter combinations

Consequently, additional analysis was conducted to evaluate how non-uniqueness affects estimates of residual subsidence. This was achieved through the evaluation of the model results, assuming low, medium, and high values of these parameters within previously estimated ranges (**Table 6**). Since an agreeable fit to the observed data could not be achieved with other reasonable values at MW-9, this analysis was only conducted at MW-5.

Table 6. Specified Aquifer Properties for MW-5 Parameter Uncertainty Analysis

Set	$K_{v\ aquitard}$ (ft/d)	$Ss_{kv\ aquitard}$ (ft $^{-1}$)	RSS (SSE)
1	3.38×10^{-6}	7.70×10^{-4}	2.34
2	1.14×10^{-5}	4.50×10^{-4}	3.58
3	5.77×10^{-5}	2.60×10^{-4}	6.74

Non-Uniqueness and Residual Subsidence at MW-5

The predicted subsidence values for Scenario 1 at time intervals 2024–2040 and 2040–2070 are detailed in **Table 7**. The simulated subsidence values shown reflect the influence of different parameter combinations—high, medium, and low values of vertical hydraulic conductivity ($K_{v\ aquitard}$) and skeletal storage coefficient ($Ss_{kv\ aquitard}$)—under Scenario 1 water level conditions (Table 6). The residual sum of

squares (RSS) error values from Table 6 show that Set 1 achieves the best fit to observed data (RSS = 2.58), while Set 3 has the highest error (RSS = 6.74). However, these RSS differences are considered very small.

Over the two time periods (2024–2040 and 2040–2070), simulated subsidence varies between the Sets. For the period 2024–2040, Set 1 predicts the highest subsidence at 3.55 feet, while Set 3 forecasts 1.94 feet. Similarly, in the 2040–2070 period, Set 1 shows 3.45 feet of subsidence, whereas Set 3 predicts just 0.84 feet. These differences underscore how parameter uncertainty affects subsidence projections: where in this case, lower $K_{v\ aquitard}$ and higher $Ss_{kv\ aquitard}$ values (Set 1) tend to produce more subsidence, while higher $K_{v\ aquitard}$ and lower $Ss_{kv\ aquitard}$ values (Set 3) lead to less subsidence.

Table 7. MW-5 Simulated Subsidence under Scenario 1

Time Period	Simulated Subsidence		
	Set 1	Set 2	Set 3
2024–2040	3.55	3.47	1.94
2040–2070	3.45	2.45	0.84

7 CONCLUSIONS AND MODEL LIMITATIONS

Model Limitations

All models contain inherent uncertainty as they are simplified representations of complex systems. Key model limitations in this study can be attributed largely to the quality and availability of data in the datasets used as input and observations in the model. These include:

- Historical water level record.
- Subsidence observations
- Drillers log (electrical log, textural log)
- Aquifer differentiation

These limitations include incomplete or poor water level records at both model sites MW-5 and MW-9, very limited subsidence observations both in quality and frequency, and variability in the accuracy of the electrical log response and subjectivity of reported textural logs. Additionally, the challenge of accurately differentiating between aquifers from limited or absent well construction information added further uncertainty.

Conclusions

Simulated subsidence at model sites MW-5 and MW-9 shows a reasonable fit with observed historical data, particularly in the period from 2007 to 2024, where data is more abundant. Both models capture subsidence trends under different water level Scenarios. Scenario 1 water levels show gradual declines in the rates of residual subsidence as water levels remain stable, while Scenario 2, which features rising water levels, shows lower rates of residual subsidence. Scenario 3, which projects prolonged water level increases, results in the lowest rates of projected residual subsidence. The predicted rates of residual subsidence are notably higher at MW-5 compared to MW-9, which is largely due to three primary factors: different stratigraphy at the two locations with a greater proportion of fine-grained (clay) sediments at

MW-5, different calibrated inelastic storage coefficients (order of magnitude lower at MW-9), and different groundwater level fluctuations (greater groundwater level declines at MW-5). The non-uniqueness of model parameters, particularly the correlation between vertical hydraulic conductivity ($K_{v\ aquitard}$) and the skeletal storage coefficient ($Ss_{kv\ aquitard}$), suggests that multiple parameter sets can yield similar model fits at MW-5, though the observed parameter behavior varies between the two model sites and was not the case at MW-9.

8 REFERENCES

Anderson, MP and Woessner, WW. 2002. Applied Groundwater Modeling: Simulation of Flow and Advective Transport. *Academic Press*, 381 p.

Boyce, SE, Hanson, RT, Ferguson, I, Schmid, W, Henson, W, Reimann, T, Mehl, SM, and Earll, MM. 2020., One-Water Hydrologic Flow Model: A MODFLOW Based Conjunctive Use and Integrated Hydrologic Flow Model (2020): US Geological Survey Techniques and Methods 6-A60, 435 p Available at: https://doi.org/10.3133/tm6a60.

Farr TG, Jones C, Liu, Z. 2015. Progress Report: Subsidence in the Central Valley, California. For Department of Water Resources by researchers at NASA's Jet Propulsion Laboratory, Pasadena, California. Available at: http://water.ca.gov/groundwater/docs/NASA_REPORT.pdf.

Faunt, CC, ed. 2009., Groundwater Availability of the Central Valley Aquifer, California: US Geological Survey Professional Paper 1766, 225 p. Available at: https://doi.org/10.3133/pp1766.

Harbaugh, AW, Banta, ER, Hill, MC, & McDonald, MG. 2000. MODFLOW-2000, The US Geological Survey (USGS) Modular Ground-Water Model-User Guide to Modularization Concepts and the Ground-Water Flow Process. Open-file Report. U. S. Geological Survey, (92), 134 p. Available at: https://doi.org/10.3133/ofr200092.

Hanson. RT. 1989. Aquifer-System compaction, Tucson Basin and Avra Valley, Arizona. US Geological Survey Water-Resources Investigations Report 88-4172, 69 p. Available at: https://doi.org/10.3133/wri884172.

Holzer, TL. 1984. Ground failure induced by ground water withdrawal from unconsolidated sediment, in Holzer, T.L., ed., Man-induced land subsidence: Geological Society of America Reviews in *Economic Geology*, v. 6, p. 67–105. Available at: https://doi.org/10.1130/REG6.

Helm, DC. 1975. One-dimensional simulation of aquifer system compaction near Pixley, California: 1. Constant parameters. *Water Resources Research* 11, 465–478 p. Available at: https://doi.org/10.1029/WR011i003p00465.

Helm, DC. 1976. One-dimensional simulation of aquifer system compaction near Pixley, California: 2. Stress Dependent parameters. Water Resources Research 12, 375–391 p. Available at: https://doi.org/10.1029/WR012i003p00375.

Hoffman, J, Leake, SA, Galloway, DL and Wilson, AM. 2003. MODFLOW-2000 ground-water model-user guide to the Subsidence and Aquifer-System Compaction (SUB) Package. US Geological Survey Open File Report 2003-233, 46 p. Available at: https://pubs.usgs.gov/of/2003/ofr03-233/.

Ireland, RL, Poland, JF, and Riley, FS. 1984. Land subsidence in the San Joaquin Valley, California, as of 1980: US Geological Survey Professional Paper 437-I. Available at: https://doi.org/10.3133/pp437I.

Jorgensen, DG. 1980. Relationships between basic soils-engineering equations and basic ground-water flow equations: US Geological Survey Water Supply Paper 2064, 40 p. Available at: https://doi.org/10.3133/wsp2064.

Leake, SA and Prudic, DE. 1991. Documentation of a computer program to simulate aquifer-system compaction using the Modular Finite Difference Groundwater Flow Model. US Geological Survey Open File Report 88-482, 68 p. Available at: https://doi.org/10.3133/twri06A2.

Lees, M, Knight, R, Smith, R. 2022. Development and Application of a 1D Compaction Model to Understand 65 Years of Subsidence in the San Joaquin Valley. Water Resources Research 58. Available at: https://doi.org/10.1029/2021WR031390.

McDonald, M and Harbaugh, AW. 1988. A Modular Three-Dimensional Finite Difference Ground-Water Flow Model. US Geological Survey Techniques of Water-Resources Investigations, Book 6, 588 p. Available at: https://doi.org/10.3133/twri06A1.

NASA Jet Propulsion Laboratory. 2019. NASA-ISRO SAR (NISAR) Mission Science Users' Handbook, California Institute of Technology, v.1, 320 p. Available at: https://nisar.jpl.nasa.gov/system/documents/files/26_NISAR_FINAL_9-6-19.pdf.

Niswonger, RG, Panday S, and Motomu, I. 2011. MODFLOW-NWT, A Newton formulation for MODFLOW-2005: US Geological Survey Techniques and Methods 6-A37, 44 p. Available at: https://doi.org/10.3133/tm6A37.

Sneed, M, Brandt, JT and Solt, M. 2018. Land subsidence along the California Aqueduct in West-Central San Joaquin Valley, California, 2003-10: US Geological Survey Scientific Investigations Report 2018-5144, 67 p. Available at: https://doi.org/10.3133/sir20185144.

Sneed, M and Galloway, DL. 2000. Aquifer-System Compaction and Land Subsidence: Measurements, Analysis and Simulations–the Holly Site, Edwards Airforce Base, Antelope Valley, California: US Geological Survey Water Investigations Report 00-4015, 65 p. Available at: https://doi.org/10.3133/wri20004015.

Terzaghi, K. 1925, Principles of soil mechanics-IV; Settlement and consolidation of clay: Erdbaumechanic, v. 95, no. 3, p. 874–878.

Traum, JA, and Faunt, CC. 2022. Central Valley Hydrologic Model version 2 (CVHM2): Groundwater Pumping: US Geological Survey data release. Available at: https://doi.org/10.5066/P9FTZ5RW.

Tre Altamira. 2021. InSAR land surveying and mapping services to DWR supporting SGMA - 2020 Update: Available at: https://data.cnra.ca.gov/dataset/tre-altamira-insar-subsidence.

Poland, J, Lofgren, B, Ireland, R, and Pugh, R. 1975. Land subsidence in the San Joaquin Valley, California, as of 1972. USGS Professional Paper 437–H. Available at: https://doi.org/10.3133/pp437H.

Sandwell, DT, Myer, D, Mellors, R, Shimada, M, Brooks, B, and Foster, J. 2008. Accuracy and resolution of ALOS interferometry: Vector deformation maps of the Father's Day Intrusion at Kilauea: IEEE Transactions on Geoscience and Remote Sensing, v. 46, no. 11, p. 3524–3534. Available at: https://doi.org/10.1109/TGRS.2008.2000634.

ADDENDUM TO 1D SUBSIDENCE MODELING REPORT

1 Introduction

An additional model scenario was run for the MW-5 location to estimate the portion of residual subsidence that may be expected to occur in the future due to water level declines that occurred between 1915 and 2015. The model inputs and results are summarized in this addendum.

2 Scenario Development

Scenario 4 for MW-5 utilizes the aquitard parameters indicated in **Table A-1**, which are calibrated aquifer and aquitard parameters equivalent to Parameter Set 1 shown in Table 6 of the 1D Subsidence Modeling Report. The groundwater levels used for Scenario 4 are shown in **Figure A-1** and are equivalent to groundwater levels used for previous Scenarios 1, 2, and 3 from 1915 to 2015. After 2015 the groundwater levels are held constant at Fall 2015 levels for Scenario 4. The calibration statistics for Scenario 4 are provided in **Table A-2** and are based on observed vs. simulated subsidence prior to 2015.

3 Scenario Results

Scenario 4 model simulation results are summarized in **Table A-3** and **Figures A-4** and **A-5**. The scenario results show that residual subsidence caused by pre-2015 groundwater level declines are estimated at 1.98 feet from 2015 to 2023, 1.95 feet from 2023 to 2040, and 2.19 feet from 2040 to 2070. Overall, these results indicate that 1.95 feet (or 55%) of the total residual subsidence estimated for Parameter Set 1 of 3.55 feet from 2023 to 2040 time period is expected to be derived from water level declines that occurred prior to 2015.

Table A-1. Calibrated Parameters at MW-5 for Scenario 4

Parameter Name	Parameter Value
	MW-5
$K_{v\ aquitard}$ (ft/d)	3.38×10^{-6}
$Ss_{kv\ aquitard}$ (ft^{-1})	7.70×10^{-4}

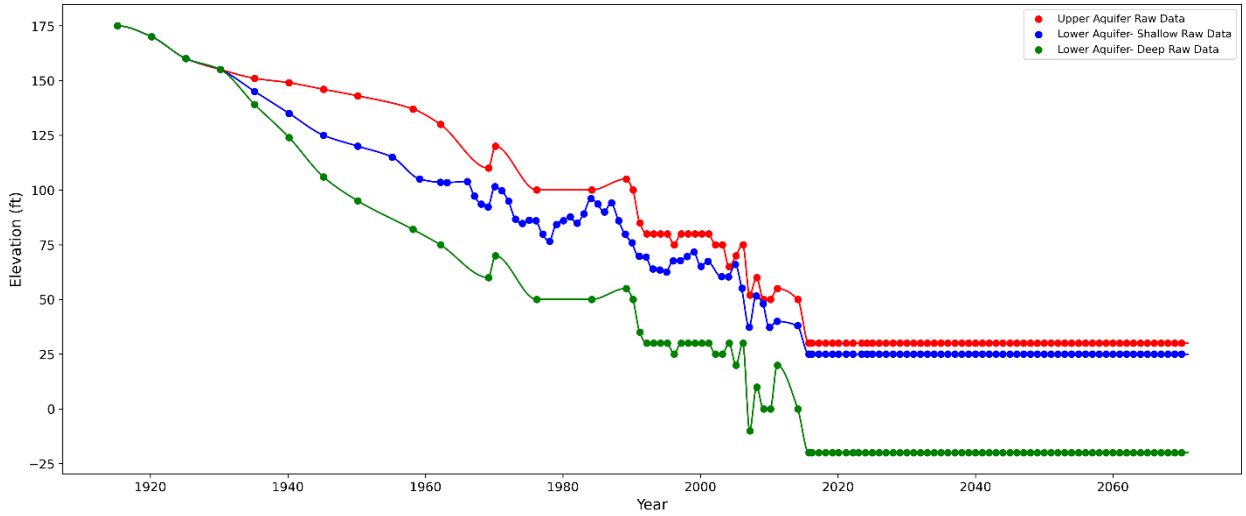

Figure A-1. Groundwater Levels Assigned in Scenario 4 for MW-5

Table A-2. MW-5 Scenario 4 Fit Statistics

Model	Statistic			
	Mean Error (ft)	Mean Absolute Error (ft)	Sum of Squared Error (ft^2)	Root Mean Squared Error (ft)
MW-5	-0.171	0.239	13.9	0.347

Table A-3. Simulated Residual Subsidence for MW-5 for Scenario 4 and Previous Scenarios for Parameter Set 1

Time Period	Simulated Subsidence				Time Period	Simulated Subsidence
	Scenario 1[1]	Scenario 2[2]	Scenario 3[3]			Scenario 4
2024–2030	1.69	1.68	1.68		2015–2023	1.98
2030–2040	1.77 (3.45)4	1.32 (3.00)	1.32 (3.00)		2023–2030	0.92 (2.9)
2040–2050	1.35 (4.81)	0.823 (3.83)	0.670 (3.67)		2030–2040	1.03 (3.93)
2050–2060	1.12 (5.93)	0.733 (4.56)	0.421 (4.10)		2040–2055	1.22 (5.15)
2060–2070	0.959 (6.89)	0.655 (5.22)	0.391 (4.49)		2055–2070	0.969 (6.12)

1. Stable water levels
2. Water level increases in 2030–2040
3. Prolonged water level increases in 2030–2040 and 2040–2055
4. Cumulative subsidence

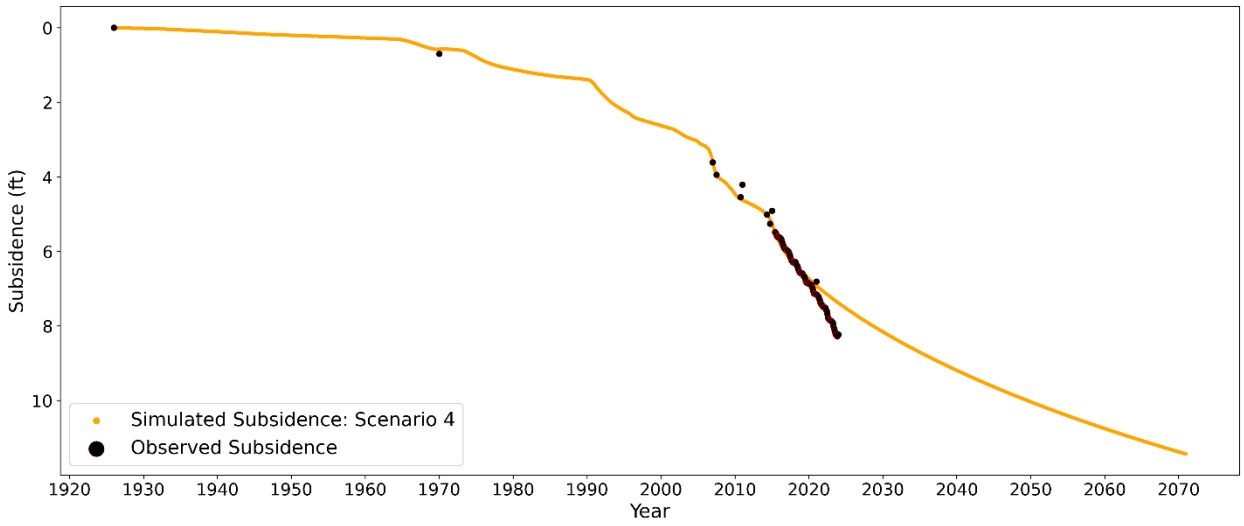

Figure A-2. Simulated Subsidence for MW-5 for Scenario 4 for Parameter Set 1

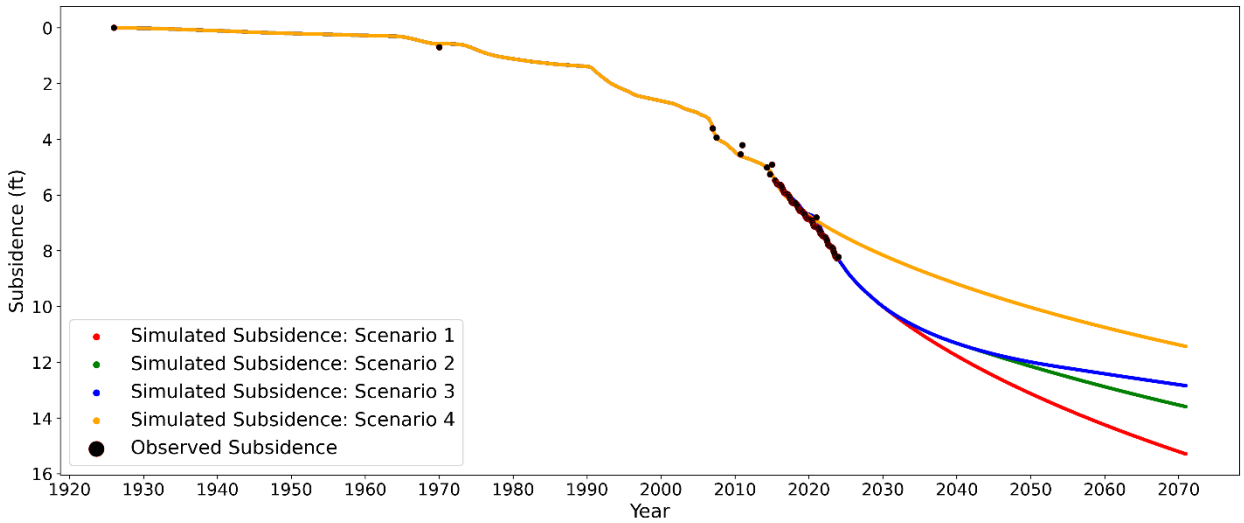

A-3. Simulated Subsidence for MW-5 for All Scenarios for Parameter Set 1